Hole magnetoplasmons in quantum dots

T. Darnhofer and U. Rössler
Institut für Theoretische Physik, Universität Regensburg, 93040 Regensburg, Germany

D. A. Broido
Department of Physics, Boston College, Chestnut Hill, Massachusetts 02167
(Received 27 November 1995)

For electrons in quantum dots the dipole absorption spectrum is known to reflect only magnetoplasmon modes with a rigid center-of-mass motion (''generalized Kohn's theorem''). A more complex behavior is expected for holes in quantum dots, as the valence-band mixing prohibits the separation of relative and center-of-mass coordinates, and the dipole field couples then also to the relative motion. We investigate theoretically the far-infrared response of hole-confining quantum dots, assuming a structure that can be realized by the lateral modulation of a two-dimensional hole gas in a $Ga_xAl_{1-x}As$-GaAs quantum well or heterojunction. The ground state of the many-hole system is determined in the local density approximation, using the 4×4 Luttinger Hamiltonian to include the valence-band mixing. The collective response to a dipole field is calculated within the random phase approximation. The resulting far-infrared absorption spectra exhibit a rich set of dipole active magnetoplasmon modes with *internal* motions of the charge density, which due to the generalized Kohn's theorem are not possible for electrons in quantum dots. [S0163-1829(96)00820-X]

I. INTRODUCTION

Recent progress in nanofabrication technology has led to the realization of semiconductor quantum dots (QD's) that confine charge carriers in all three spatial directions. Such structures have been made by superimposing a lateral modulation onto an otherwise two-dimensional electron gas (2DEG) in quantum wells (QW's) or heterojunctions (HJ's). Despite the complexity of the confined many-electron systems—which sometimes are addressed as ''artificial atoms''—QD's exhibit a rather simple far-infrared (FIR) dipole absorption spectrum, even in the presence of a magnetic field.[1–7] This has been explained as being a consequence of the parabolic lateral confinement potential and of the parabolic conduction band characterized by an effective mass m^*. In this case the FIR absorption spectrum shows the single-particle spectrum of the center-of-mass (c.m.) motion, because the dipole operator depends only on the c.m. coordinates, which can be separated from the relative coordinates. Thus, the dipole spectra do not exhibit the many-particle interaction, a fact known as the ''generalized Kohn's theorem'' (GKT).[8–11] The dipole resonances are those of the 2D harmonic oscillator in a magnetic field[12–14]

$$\omega_{\pm}=\sqrt{\omega_0^2+\left(\frac{\omega_c}{2}\right)^2}\pm\frac{\omega_c}{2}, \tag{1}$$

where ω_0 is the lateral confinement frequency, and $\omega_c=eB/m^*$ the cyclotron frequency. These collective excitations are magnetoplasmon modes with a rigid c.m. motion against the neutralizing charged background. Deviations from this simple two-mode absorption spectrum can be induced by nonparabolicities in the lateral confinement potential or by band-structure effects.

For two and three electrons in a QD with nonparabolic confinement exact calculations of the dipole spectra have been performed.[15–18] The resulting specific splittings of the modes $\omega_{\pm}$ can be compared qualitatively to weak features in the observed FIR spectra of QD's with a controllable number of very few electrons per dot.[5] For higher numbers of electrons per QD the FIR spectra have been described in the Hartree and the Hartree-Fock approximation.[7,17–20] The collective excitations obtained within these theories give magnetoplasmon modes with frequencies $\omega_{\pm}$ as in Eq. (1) and small splittings that are induced by nonparabolicities in the confinement. Calculations within a classical hydrodynamic model give magnetoplasmon modes where the lowest frequencies again have the magnetic field dependence of $\omega_{\pm}$ in Eq. (1).[21,22] It has been shown that even for highly nonparabolic confinement the dipole absorption is dominated by these two modes and higher modes become only weakly dipole active.[22]

Band-structure effects have been detected for electrons in QD's on InSb,[1,6] whose conduction band deviates significantly from the simple parabolic form. Calculations that take into account this nonparabolicity[23–25] are in quantitative agreement with the observed downward shift of the ω_+ mode. For InSb QD's with high lateral quantization energies, comparable to the energy separation of the states in growth direction, coupling of these states must also be considered to obtain agreement between theory and experiment.[6] Specific line splittings due to band nonparabolicity and spin-orbit coupling have been predicted theoretically for QD's in InSb,[24] but these splittings are smaller than the resolution of the available experiments.[1,6]

Much stronger effects can be expected for holes in quantum dots[23,26–28] from the complex structure of the valence band.[29–32] It is known from experimental and theoretical investigations of 2D hole gases (2DHG's) in $Ga_xAl_{1-x}As$-GaAs HJ's (Refs. 33–40) and Ge-SiGe QW's (Refs. 41–44) that the degeneracy of the bulk valence band causes particular features: the coupling between heavy-hole

(HH) and light-hole (LH) states leads to unequally spaced hole Landau levels with a highly nonlinear magnetic field dispersion, which results in complex cyclotron resonance spectra. The HH-LH coupling prohibits an application of Kohn's theorem: it has been shown that many-body effects have an influence on the dipole excitation of hole magnetoplasmons in 2DHG's.[45] Calculations of the eigenenergies of a single hole in a QD (Refs. 23 and 26) and of the corresponding single-particle dipole spectrum[27] have already demonstrated the strong impact of the HH-LH coupling for holes in QD's. In a recent work[28] we have published results for collective excitations of many holes in a QD, which show significant deviations from the simple behavior of electrons in QD's governed by the GKT.

The outline of this paper is as follows: In Sec. II we present Luttinger's 4×4 $\mathbf{k}\cdot\mathbf{p}$ Hamiltonian, which is used to take the valence-band structure into account. In Sec. III we describe the determination of the ground state of holes in a QD within the local density approximation (LDA). In Sec. IV we present calculations in the time-dependent LDA or random phase approximation (RPA) to describe the collective electromagnetic response of the system and the excitation of magnetoplasmons by an external dipole field. In Sec. V the model parameters are given for QD structures assumed to be realized by the lateral modulation of the 2DHG in a $Ga_xAl_{1-x}As$-GaAs QW or HJ. In Sec. VI we show the calculated FIR absorption spectra for these two systems, which are clearly distinct due to the different symmetry in growth direction. We present motion patterns of the charge density for dipole active hole magnetoplasmon modes, which are significantly more complex than the known c.m. motion of electrons in QD's governed by the GKT.

II. VALENCE-BAND STRUCTURE

To describe the Γ_8^v valence band with hole spin $m_j = \pm 3/2$ for HH and $m_j = \pm 1/2$ for LH we use Luttinger's 4×4 $\mathbf{k}\cdot\mathbf{p}$ Hamiltonian within the axial approximation, neglecting the small anisotropy of the in-plane band structure. For the basis order $m_j=(+3/2,+1/2,-1/2,-3/2)$ it has the form[29]

$$H_L=\begin{pmatrix} P+Q+\frac{3}{2}\kappa B & S & R & 0 \\ S^\dagger & P-Q+\frac{1}{2}\kappa B & 0 & R \\ R^\dagger & 0 & P-Q-\frac{1}{2}\kappa B & -S \\ 0 & R^\dagger & -S^\dagger & P+Q-\frac{3}{2}\kappa B \end{pmatrix}, \tag{2}$$

$$P=\frac{\gamma_1}{2m_0}(p_x^2+p_y^2+p_z^2)=:P_{xy}+P_z, \tag{3a}$$

$$Q=\frac{\gamma_2}{2m_0}(p_x^2+p_y^2)-\frac{2\gamma_2}{2m_0}p_z^2=:Q_{xy}+Q_z, \tag{3b}$$

$$R=\frac{\gamma_2+\gamma_3}{2m_0}(-\sqrt{3}/2)(p_x-ip_y)^2, \tag{3c}$$

$$S=\frac{\gamma_3}{2m_0}(-2\sqrt{3})(p_x-ip_y)p_z. \tag{3d}$$

The diagonal contributions $P\pm Q$ are the kinetic energy operators for uncoupled HH's and LH's with respective in-plane masses $m_0/(\gamma_1\pm\gamma_2)$ and z masses $m_0/(\gamma_1\mp2\gamma_2)$. In Eqs. (3a) and (3b) we separate P and Q into operators that depend only on p_x and p_y or only on p_z. The off-diagonal parts R and S couple HH and LH states. A magnetic field in the z direction $\mathbf{B}=(0,0,B)$ is included by defining the differential operators $\mathbf{p}=-i\hbar\nabla+e\mathbf{A}$ with a vector potential in the symmetric gauge $\mathbf{A}=B/2(-y,x,0)$. The Zeeman splitting is given by the terms $m_j\kappa B$ on the diagonal of H_L.

The Hamiltonian H_L of Eq. (2) has been used in Refs. 36 and 38–40 to describe a 2DHG in a perpendicular magnetic field. The HH-LH mixing couples the in-plane motion to the motion in growth direction, which leads to highly nonparabolic 2D subbands and to a strong mixing of Landau levels evolving from different subbands. In Refs. 23, 26 and 27 we have used H_L to model the properties of a single hole in a QD and demonstrated the importance of HH-LH coupling for holes in QD's.

III. GROUND STATE

For our calculations we use a confinement potential with axial symmetry. We employ a cylindrical coordinate system with a 3D vector $\mathbf{r}=(x,y,z)$ written as $\mathbf{r}=(\boldsymbol{\rho},z)$, where $\boldsymbol{\rho}=(\rho,\varphi)$ is a 2D vector in polar coordinates. The confinement is modeled by a superposition of a potential $V_z(z)$ in the growth direction and a parabolic lateral potential $V_{xy}(\rho)=\frac{1}{2}K_0\rho^2$. This form is in good agreement with calculations that model the electrostatic potential in QD's.[46–48] Small nonparabolicities in $V_{xy}(\rho)$ could easily be incorporated in the following calculations but shall be neglected here, as their known influence on the dipole

excitations[7,15–20,22] is much weaker than the effects induced by the valence-band structure. For realistic QD systems the confinement in the x-y plane is much wider than that in the z direction. This results in quite different energy separations of the quantized levels associated with these confinements, and in a very flat, disklike electron or hole system.

We describe the many-hole ground state of the QD in the LDA. The effective single-particle potential is added to the diagonal of H_L in Eq. (2). The total Hamiltonian of our system is then given by

$$H = H_L + \mathbb{1}_{4\times 4}[V_z(z) + V_{xy}(\rho) + V_H(\mathbf{r}) + V_{\mathrm{XC}}(\mathbf{r})], \quad (4)$$

where $V_H(\mathbf{r})$ is the Hartree potential and $V_{\mathrm{XC}}(\mathbf{r})$ the exchange-correlation potential.

Due to the axial symmetry of H_L in Eq. (2) and of the confinement potential, the z component of total angular momentum is a good quantum number. The wave functions can then be labeled by the corresponding quantum number M and a second index μ,

$$\Psi_{M\mu}(\mathbf{r}) = \sum_{m_j=-3/2}^{+3/2} u_{m_j}(\mathbf{r}) F_{m_j}^{M\mu}(\mathbf{r}), \quad (5)$$

and are sums over products of bulk band edge Bloch functions $u_{m_j}(\mathbf{r})$ and envelope functions $F_{m_j}^{M\mu}(\mathbf{r})$. We expand the envelope functions in terms of products of the eigenfunctions of $P_z \pm Q_z + V_z(z)$ and the wave functions of the 2D harmonic oscillator in the x-y plane. The two different masses in the z direction, $m_0/(\gamma_1 - 2\gamma_2)$ for HH and $m_0/(\gamma_1 + 2\gamma_2)$ for LH, give rise to two different sets of wave functions, which we label by $\zeta_{|m_j|\nu}(z)$ with $\nu = 1,2,\ldots$ and $|m_j| = 3/2$ for HH, $|m_j| = 1/2$ for LH. As it will turn out later, it is advantageous to define the 2D oscillator in the x-y plane for the mass m_0/γ_1 by using the hybrid frequency $\sqrt{\omega_0^2 + (\omega_c/2)^2}$ with $\omega_0^2 = K_0\gamma_1/m_0$ and $\omega_c = eB\gamma_1/m_0$, which corresponds to the Hamiltonian $P_{xy} + V_{xy}(\rho)$. (The term Q_{xy} will be considered later.) The corresponding wave functions are of the form $R_{n|m|}(\rho)e^{im\varphi}$, where m is the orbital angular momentum, and n the radial quantum number. The explicit form of the radial functions $R_{n|m|}(\rho)$ of the 2D harmonic oscillator is given, for example, in Ref. 13. The expansion in the chosen basis is then written as

$$F_{m_j}^{M\mu}(\mathbf{r}) = \sum_{\nu n} C_{m_j}^{M\mu}(\nu, n)\zeta_{|m_j|\nu}(z) R_{n|M-m_j|}(\rho) e^{i(M-m_j)\varphi}, \quad (6)$$

where the values for the respective orbital angular momenta are fixed to $m = M - m_j$ due to the conservation of the total angular momentum. For every value of M, the mixing coefficients $C_{m_j}^{M\mu}(\nu, n)$ are determined by numerical diagonalizations of the full Hamiltonian with off-diagonal terms Q_{xy}, R, and S of H_L in Eq. (2), and $V_H(\mathbf{r}) + V_{\mathrm{XC}}(\mathbf{r})$ of Eq. (4). The corresponding eigenvalues give the energies $E_{M\mu}$. For the chosen basis, the matrix elements for Q_{xy}, R, and S can easily be evaluated analytically by expressing these differential operators in terms of the creation and annihilation operators of the 2D harmonic oscillator.[49] The mass deviation term Q_{xy} is diagonal in m_j and ν, but R and S are off diagonal and couple HH and LH states.

The occupation of the lowest levels is given by the Fermi function $f(E_{M\mu})$ and the ground-state density is

$$n(\mathbf{r}) = \sum_{M\mu} f(E_{M\mu}) \sum_{m_j=-3/2}^{+3/2} |F_{m_j}^{M\mu}(\mathbf{r})|^2 = \sum_{m_j=-3/2}^{+3/2} n_{m_j}(\mathbf{r}), \quad (7)$$

where $F_{m_j}^{M\mu}(\mathbf{r})$ are the envelope functions of Eq. (6). The ground-state density can be decomposed into contributions $n_{m_j}(\mathbf{r})$ from the four spinor components. The modulation of the wave functions $\Psi_{M\mu}(\mathbf{r})$ in Eq. (5) by the Bloch functions $u_{m_j}(\mathbf{r})$ is neglected in the usual envelope function approximation by averaging over the unit cells of the lattice and exploiting the orthogonality of the $u_{m_j}(\mathbf{r})$. To evaluate the Hartree potential

$$V_H(\mathbf{r}) = \frac{e^2}{\varepsilon}\int \rho' d\rho' \int d\varphi' \int dz' \frac{n(\mathbf{r}')}{|\mathbf{r} - \mathbf{r}'|} \quad (8)$$

we exploit the very flat disklike shape of the charge density and approximate in Eq. (8) $|\mathbf{r} - \mathbf{r}'| \approx |\boldsymbol{\rho} - \boldsymbol{\rho}'|$. Then the z' integration in Eq. (8) can be used to define a 2D density with axial symmetry $n(\rho') = \int dz' n(\mathbf{r}')$ and the φ' integration reduces Eq. (8) to the 1D integral

$$V_H(\rho) = \frac{e^2}{\varepsilon}\int d\rho' \rho' n(\rho') \frac{4}{\rho_>} K\left(\frac{\rho_<}{\rho_>}\right), \quad (9)$$

where

$$\rho_> = \begin{Bmatrix} \rho \\ \rho' \end{Bmatrix}, \quad \rho_< = \begin{Bmatrix} \rho' \\ \rho \end{Bmatrix} \text{ for } \begin{Bmatrix} \rho > \rho' \\ \rho < \rho' \end{Bmatrix}, \quad (10)$$

and K is the complete elliptic integral of the first kind.

In Refs. 36–40, 43, and 44 the 2DHG's were described only within the Hartree approximation. In a recent publication[50] a density-functional approach for holes was presented: the exchange and correlation energies were calculated for a homogeneous 3D hole gas, including the degeneracy of the bulk valence band. In the case of 2DHG's with strong quantum confinement in the growth direction the energy separation between the first HH subband and the other subbands is large. For realistic QD parameters, the occupied hole states evolve from this first HH subband and the density has mainly HH character with only a small LH contribution due to HH-LH coupling. Therefore, we do not use an exchange-correlation potential derived from the degenerate bulk valence band as in Ref. 50, but take an exchange-correlation potential for a 2DEG and scale it with the in-plane HH mass $m_0/(\gamma_1 + \gamma_2)$. In the standard way, we take

$$V_{\mathrm{XC}}(n) = \frac{d}{dn}\{n[E_X(n) + E_C(n)]\}, \quad (11)$$

where $E_X(n)$ and $E_C(n)$ are the exchange and correlation energy as a function of the homogeneous density n of a 2DEG, taken from the calculations of Ref. 51. A possible magnetic field dependence of $E_X(n)$ and $E_C(n)$ is neglected.

The matrix elements of $V_H(\rho)+V_{\rm XC}(\rho)$ between the radial functions $R_{n|m|}(\rho)$ are calculated numerically employing a modified Simpson's quadrature to account for the weak singularity of K in Eq. (9). These contributions are diagonal in m_j and ν, but mix states with different radial quantum numbers n. Self-consistency of the ground state is achieved in an iterative procedure.

IV. ELECTROMAGNETIC RESPONSE

The standard experimental setup for FIR spectroscopy on QD's involves an electromagnetic wave propagating in the z direction (perpendicular to the QD array) with the vector of the electric field in the x-y plane. This is described by a time-dependent external potential $e\Phi^{\rm ex}(\mathbf{r},t)=V^{\rm ex}(\boldsymbol{\rho})e^{i\omega t}$, where $V^{\rm ex}(\boldsymbol{\rho})$ contains the information about the polarization. The linear response to this perturbation is described using the density-density correlation function, or susceptibility

$$\chi(\mathbf{r},\mathbf{r}',\omega)=\sum_{M\mu M'\mu'}\frac{f(E_{M\mu})-f(E_{M'\mu'})}{\hbar\omega+E_{M\mu}-E_{M'\mu'}+i\Gamma}\times\Psi^*_{M\mu}(\mathbf{r})\Psi_{M'\mu'}(\mathbf{r})\Psi^*_{M'\mu'}(\mathbf{r}')\Psi_{M\mu}(\mathbf{r}'),\quad(12)$$

where Γ is a phenomenological broadening factor. We again use the envelope function approximation to average over the unit cells of the semiconductor lattice and exploit the orthogonality of the Bloch functions $u_{m_j}(\mathbf{r})$ in the wave functions $\Psi_{M\mu}(\mathbf{r})$ of Eq. (5). The susceptibility $\chi(\mathbf{r},\mathbf{r}',\omega)$ is then determined by the envelope functions $F^{M\mu}_{m_j}(\mathbf{r})$ of Eq. (6) and the eigenenergies $E_{M\mu}$. Analogous to Sec. III we restrict our model to a 2D description of the very flat disklike charge density by taking $|\mathbf{r}-\mathbf{r}'|\approx|\boldsymbol{\rho}-\boldsymbol{\rho}'|$. The induced change of the 2D density $\delta n(\boldsymbol{\rho},\omega)=\int dz\,\delta n(\mathbf{r},\omega)$ is then given by the RPA formula[19,52]

$$\delta n(\boldsymbol{\rho},\omega)=\int d\boldsymbol{\rho}'\chi(\boldsymbol{\rho},\boldsymbol{\rho}',\omega)\left[V^{\rm ex}(\boldsymbol{\rho}')+\frac{e^2}{\varepsilon}\int d\boldsymbol{\rho}''\frac{\delta n(\boldsymbol{\rho}'',\omega)}{|\boldsymbol{\rho}'-\boldsymbol{\rho}''|}+\left(\frac{\partial V_{\rm XC}}{\partial n}\right)\delta n(\boldsymbol{\rho}',\omega)\right],\quad(13)$$

where $\chi(\boldsymbol{\rho},\boldsymbol{\rho}',\omega)=\int dz\int dz'\,\chi(\mathbf{r},\mathbf{r}',\omega)$ is the 2D susceptibility. The first term in the bracket of the right-hand side of Eq. (13) stands for the bare external dipole field, which is screened by the two following terms. The resulting respective shifts of the collective resonances are known as ''depolarization shift'' and ''excitonic shift.''

Following Ref. 19, we take advantage of the axial symmetry of the system and expand

$$V^{\rm ex}(\boldsymbol{\rho})=\sum_l e^{il\varphi}V^{\rm ex}_l(\rho),\quad(14a)$$

$$\delta n(\boldsymbol{\rho},\omega)=\sum_l e^{il\varphi}\delta n_l(\rho,\omega),\quad(14b)$$

$$\chi(\boldsymbol{\rho},\boldsymbol{\rho}',\omega)=\sum_l e^{il(\varphi-\varphi')}\chi_l(\rho,\rho',\omega).\quad(14c)$$

This allows us to decompose Eq. (13) into separate equations for components with different angular symmetry l. With the 2D Fourier expansion of $1/|\boldsymbol{\rho}'-\boldsymbol{\rho}''|$ we get

$$\delta n_l(\rho,\omega)=\int d\rho'\rho'\Big[\chi_l(\rho,\rho',\omega)V^{\rm ex}_l(\rho')+\beta_l(\rho,\rho',\omega)\,\delta n_l(\rho',\omega)+\chi_l(\rho,\rho',\omega)\times 2\pi\left(\frac{\partial V_{\rm XC}}{\partial n}\right)\delta n_l(\rho',\omega)\Big],\quad(15)$$

with

$$\beta_l(\rho,\rho',\omega)=\frac{4\pi^2e^2}{\varepsilon}\int d\rho''\rho''\chi_l(\rho,\rho'',\omega)R_l(\rho',\rho''),\quad(16)$$

$$R_l(\rho',\rho'')=\int dq J_l(q\rho')J_l(q\rho''),\quad(17)$$

where J_l denotes the Bessel functions.

To describe an electric dipole field of strength $E^{\rm ex}$ with circular polarization we set in Eq. (14a)

$$V^{\rm ex}_l(\rho)=\begin{cases}eE^{\rm ex}\rho, & l=\pm1,\\ 0, & l\neq\pm1,\end{cases}\quad(18)$$

where $\pm$ stands for the two polarization directions. Thus, only magnetoplasmon modes with $l=\pm1$ couple to the external dipole radiation. For $|l|=1$ the integral in Eq. (17) gives

$$R_{\pm1}(\rho,\rho')=\frac{2}{\pi}\frac{1}{\rho_<}\left[K\left(\frac{\rho_<}{\rho_>}\right)-E\left(\frac{\rho_<}{\rho_>}\right)\right],\quad(19)$$

where K and E denote the complete elliptic integrals of the first and second kind, respectively, and $\rho_<$ and $\rho_>$ as defined in Eq. (10). We solve the integral equation Eq. (15) for $\delta n_l(\rho,\omega)$ for $l=+1$ and $l=-1$ on a discrete grid for the variable ρ by direct matrix inversion, employing the same quadrature as in Sec. III.

The time dependence of the induced change of the density is

$$\delta n(\boldsymbol{\rho},t)=\frac{1}{2\pi}\delta n(\boldsymbol{\rho},\omega)e^{-i\omega t}=\frac{1}{2\pi}\delta n_{\pm1}(\rho,\omega)e^{i(\pm\varphi-\omega t)},\quad(20)$$

which gives the plasmonic motion of the charge density for the two polarization directions. From $\delta n(\boldsymbol{\rho},\omega)$ we can also calculate the polarizability

$$\alpha_\pm(\omega)=\frac{1}{E^{\rm ex}}\int d\boldsymbol{\rho}\rho e^{\pm i\varphi}\delta n(\boldsymbol{\rho},\omega)=\frac{2\pi}{E^{\rm ex}}\int d\rho\rho^2\delta n_{\pm1}(\rho,\omega),\quad(21)$$

and the cross section for photon absorption

$$\sigma_{\pm}(\omega)=4\pi\frac{\omega}{c}\mathrm{Im}\{\alpha_{\pm}(\omega)\}, \tag{22}$$

which describes the observable FIR absorption for the two polarization directions.

V. MODEL PARAMETERS

As QD's with holes have not yet been fabricated, we assume realistic model parameters for our calculation. The most likely starting point for the realization of such a QD structure is the 2DHG in a $Ga_{1-x}Al_xAs$-GaAs QW or HJ.[33–40] Therefore, we use the Luttinger parameters and the dielectric constant for GaAs ($\gamma_1 = 6.85$, $\gamma_2 = 2.1$, $\gamma_3 = 2.9$, $\kappa = 1.2$, and $\varepsilon = 13.1$).[53] To describe a $Ga_{1-x}Al_xAs$-GaAs QW structure, we use a rectangular potential well for $V_z(z)$. We choose a well width of 100 Å and an Al content in the barrier of $x = 0.3$, which gives a valence-band offset of 130 meV. For these QW parameters the eigenenergies for the first and second subband functions $\zeta_{|m_j|\nu}(z)$ are 7.4 and 29.5 meV for HH, and 20.2 and 78.0 meV for LH. For the HJ, we use for $V_z(z)$ a triangular potential[54,55] with an infinite offset for $z<0$ and a constant electric field for $z>0$. To allow a comparison with the QW system, we chose an electric field of 0.265 mV/Å, which leads to subband energies of 20.8 and 36.4 meV for HH, and 33.6 and 58.7 meV for LH and gives the same separation between the first HH subband and the first LH subband of 12.8 meV as in the QW system. This chosen value for HH-LH subband separation is in agreement with the known data for the 2D hole systems in $Ga_xAl_{1-x}As$-GaAs HJ's.[33–40]

For the matrix elements of the HH-LH coupling terms R and S, integrals with the functions $\zeta_{|m_j|\nu}(z)$ of the form $\int dz\zeta_{1/2\nu}(z)\zeta_{3/2\nu'}(z)$, and $\int dz\zeta_{1/2\nu}(z)p_z\zeta_{3/2\nu'}(z)$ have to be evaluated. For the QW half of these matrix elements are zero due to the inversion symmetry in the z direction and the total matrix separates into two blocks. The lack of this symmetry for the HJ leads to additional couplings.

To determine the curvature of the lateral potential $V_{xy}(\rho)=\frac{1}{2}K_0\rho^2$, we assume a similar electrostatic modulation as for the GaAs QD's with electrons from Refs. 2, 3, and 7, where a confinement frequency of about 4 meV was observed. To scale this for the used oscillator mass m_0/γ_1, we take $\hbar\omega_0=\hbar\sqrt{K_0\gamma_1/m_0}$ = (4 meV) $\sqrt{\gamma_1 m^*}$= 2.6 meV, where $m^* = 0.067m_0$ is the effective electron mass of GaAs. With the mass deviation term Q_{xy} this leads to an oscillator spacing of 3.0 meV for HH and 2.2 meV for LH. The calculations have been made for a temperature of $T = 1.0$ K. For the phenomenological line broadening in Eq. (12) we use $\Gamma = 0.1$ meV.

In the investigated range of up to 14 holes per QD convergence for the calculated FIR absorption spectra was achieved by including in the basis for the expansion of the wave functions in Eq. (5) the first two functions $\zeta_{|m_j|\nu}(z)$, $\nu = 1,2$ for HH ($m_j=\pm 3/2$) and LH ($m_j=\pm 1/2$) and the eleven lowest radial functions $R_{n|m|}(\rho)$ for $n = 0,1,\ldots,10$. The total matrix size for a diagonalization was therefore 88 × 88. To determine the ground state, the diagonalization had to be performed for several total angular momenta M.

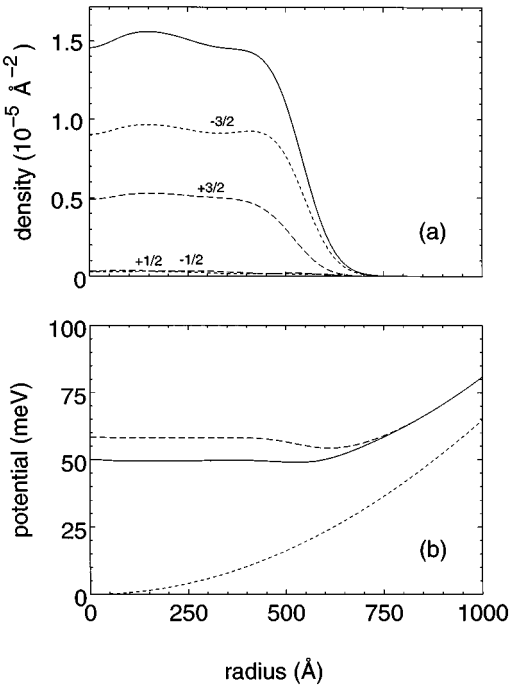

FIG. 1. Self-consistent ground state at $B = 4$ T for 14 holes in a quantum dot based on a $Ga_xAl_{1-x}As$-GaAs heterojunction: (a) solid line: total density; dashed lines: the contributions of the four spinor components with hole spin $m_j = +3/2, +1/2, -1/2, -3/2$. (b) dotted line: external parabolic confinement; dashed line: external confinement plus Hartree potential; solid line: total potential, including the exchange-correlation potential.

VI. RESULTS

In Fig. 1 we display as an example the self-consistent ground-state density and the potential for 14 holes in a QD based on a HJ for a magnetic field of $B = 4$ T. In Fig. 1(a) the density $n(\rho)$ is shown with a solid line. According to Eq. (7) it is the sum over the contributions $n_{m_j}(\rho)$ of the four hole spin components, which are shown separately by dashed lines. The two HH components are much bigger than the two LH components. For 14 holes in the QD we get a 2D hole density of around 1.5×10^{11} cm^{-2} in the center of the dot, which is in the order of magnitude known for 2DHG's in $Ga_xAl_{1-x}As$-GaAs HJ's.[33–40] From Fig. 1(a) we estimate the diameter of the disklike charge density to be about 1200 Å, which is substantially bigger than the extension in the z direction of about 100 Å (for the QW, as well as for the HJ parameters). This demonstrates the validity of the 2D approximation that was used in the ground state and response calculations in the present work and throughout the existing theoretical literature on FIR spectra of QD's with electrons.[7,15–20, 22]

Figure 1(b) displays the radial potential, corresponding to the density of Fig. 1(a). The external parabolic confinement $V_{xy}(\rho)$ is shown with the dotted line, the dashed line gives $V_{xy}(\rho)$ plus the Hartree potential $V_H(\rho)$, the solid line gives the total potential $V_{xy}(\rho)+V_H(\rho)+V_{XC}(\rho)$ including the exchange-correlation potential. The screening of the confinement potential due to the charge carriers in the center of the QD leads to a flat bottom of the effective single-particle potential. The upward shift of the potential bottom (of about 50

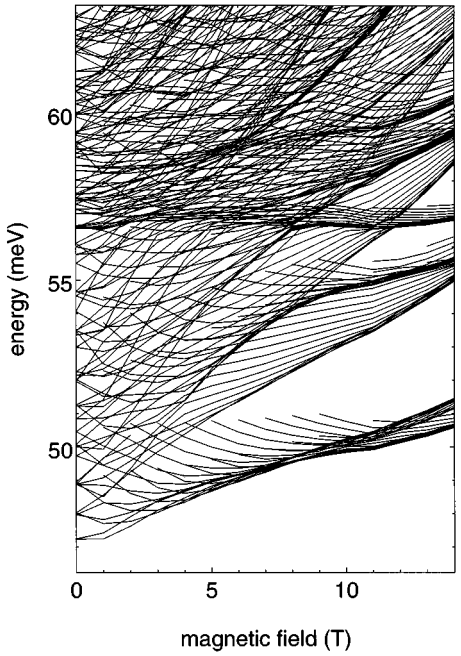

FIG. 2. Eigenenergies as a function of the magnetic field for six holes in a quantum dot based on a $Ga_xAl_{1-x}As$-GaAs heterojunction. (Hole energies are taken positive.)

meV for 14 holes) gives the estimate for the interaction energy of the system within our mean-field description.

In Fig. 2 we show selected lowest eigenenergies $E_{M\mu}$ as a function of the magnetic field B for the case of 6 holes in a QD based on a HJ. The levels lie above an energy that is given by the addition of the energy from the quantization in the z direction (of 20.8 meV for the lowest HH subband) and the upward shift of the potential bottom by the Hartree and exchange-correlation potential (of about 25 meV for 6 holes). Due to the flat bottom of the self-consistent potential the level spacing is significantly smaller than the confinement frequency for HH of 3.0 meV. At $B = 0$ states with total angular momentum $+M$ and $-M$ are degenerate. For small B, the $m_j = -3/2$ states[58] are lower than those with $m_j = +3/2$ due to the Zeeman term $m_j \kappa B$. With increasing B, the HH-LH coupling lowers the $+3/2$ states relative to their $-3/2$ counterparts. This leads to a crossing of these two sets of states at $B = 7-8$ T. In the high magnetic field limit the QD levels converge into hole Landau levels and the lowest states belong to a Landau level with dominant $m_j = +3/2$ character. To illustrate this B dependence of the ground-state character, we have plotted in Fig. 3 the integrals $(1/N)\int d\mathbf{r}\, n_{m_j}(\mathbf{r})$ over the density components of Eq. (7), normalized by the number of holes $N = 6$. We see, that in the whole magnetic field range the occupied states have mainly HH character (dominated by $m_j = -3/2$ below 8 T and by $+3/2$ above 8 T) with only very small LH contributions ($m_j = \pm 1/2$). As already mentioned in Sec. III, this justifies our approximation for an exchange-correlation potential derived for a 2DEG, scaled with the HH in-plane mass.

In two recent papers[56,57] it has been shown that the time-dependent LDA can reproduce the exact result of the GKT. This has also been found in Refs. 7 and 18–20, where the Hartree-RPA calculations for electrons in QD's with parabolic confinement give the known simple two-mode absorption spectrum with the resonance frequencies $\omega_\pm$ of Eq. (1) for the plasmonic c.m. motion. If we artificially set the HH-LH coupling terms R and S in H_L of Eq. (2) to zero, our system reduces to the simple one known for electrons, but with the HH in-plane mass $m_0/(\gamma_1+\gamma_2)$ as only states evolving from the lowest HH subband are occupied. In Fig. 4 we show the corresponding FIR absorption $\sigma_\pm(\omega)$ for the two polarization directions of circular polarized radiation. Within an error of less than 1%, the result is in agreement with Eq. (1), applied to the mass $m_0/(\gamma_1+\gamma_2)$ and the oscillator frequency $\hbar\omega_0 = 3.0$ meV. It should be noted that even in the absence of band mixing, HH's and LH's are coupled by the Coulomb interaction. As a result, a QD system containing uncoupled HH's *and* LH's would not satisfy Kohn's theorem, and the resulting spectrum would be more complicated than the one in Fig. 4.[28]

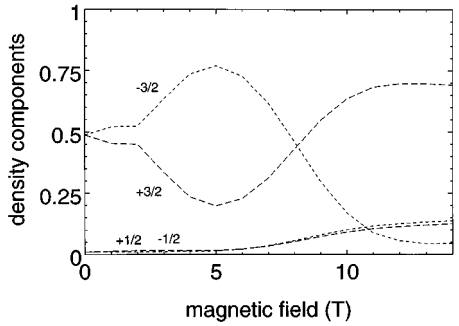

FIG. 3. Integrated density components for hole spin $m_j = +3/2, +1/2, -1/2, -3/2$ as a function of the magnetic field for six holes in a quantum dot based on a $Ga_xAl_{1-x}As$-GaAs heterojunction. The ground state has mainly heavy-hole character, dominated by $m_j = -3/2$ below 8 T, and by $m_j = +3/2$ above 8 T.

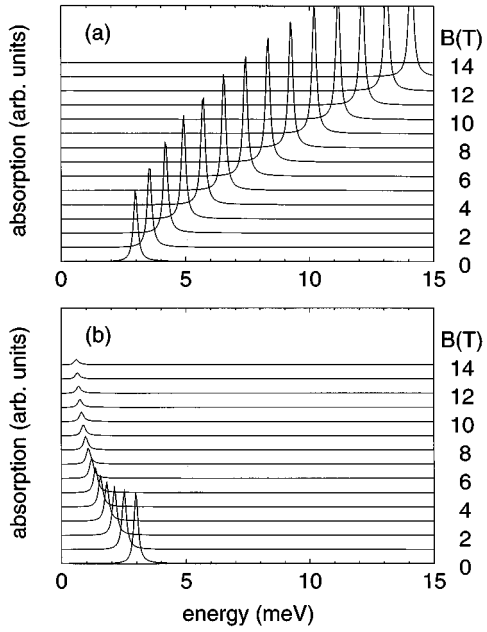

FIG. 4. Absorption spectrum for (a) the plus, and (b) the minus direction of circular polarization for holes in quantum dots *without* the heavy-hole light-hole coupling terms R and S. Neglecting these couplings reduces the system to the one with electrons.

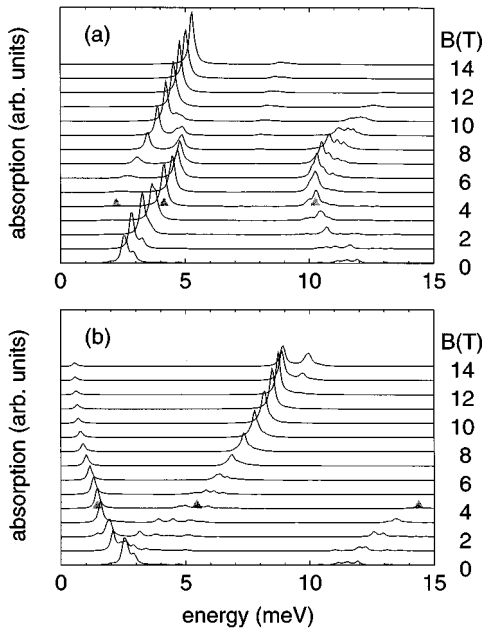

FIG. 5. Absorption spectrum for 14 holes in a quantum dot based on a $Ga_xAl_{1-x}As$-GaAs heterojunction for (a) the plus polarization, and (b) the minus polarization. The strong deviations from the spectrum in Fig. 4 are induced by heavy-hole light-hole coupling. For the resonances marked with the grey triangles, the plasmonic motions of the density are shown in Fig. 8.

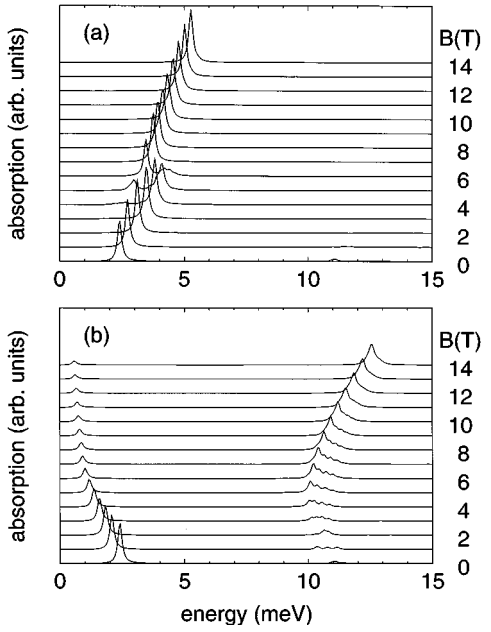

FIG. 6. Same as in Fig. 5, but for a quantum dot based on a $Ga_xAl_{1-x}As$-GaAs quantum well. The inversion symmetry in the growth direction leads to a simpler absorption spectrum as in the case of a heterojunction shown in Fig. 5.

The FIR absorption for 14 holes in a QD based on the HJ, calculated *with* the HH-LH coupling terms R and S is shown in Fig. 5. The important effect of this coupling becomes evident by comparison with Fig. 4. The dominant mode in the plus polarization [see Fig. 5(a)] has a much weaker magnetic field dispersion and a large splitting for $B=6-9$ T. The magnetic field dispersion results from the repulsion between levels due to HH-LH coupling and is found already in the corresponding single particle excitations.[27] The splitting is a consequence of the changing occupation of the lowest levels described above and illustrated in Fig. 3: at small magnetic fields $B<6$ T the spectrum is dominated by transitions originating from the states with $m_j=-3/2$ character,[58] whereas for $B>11$ T transitions from the $+3/2$ states are important. At intermediate fields $B=7-10$ T both kinds of transitions are possible, which leads to the splitting. A new mode appears in the plus polarization for magnetic fields $B<10$ T at an energy around 11 meV, which is related to the separation between the first HH and first LH subband of 12.8 meV. This ''inter-subband mode'' becomes dipole allowed as the $\mathbf{k}\cdot\mathbf{p}$ Hamiltonian H_L of Eq. (2) couples the levels evolving from different subbands in the z direction. For the minus polarization [see Fig. 5(b)] we find a basically unchanged ω_- mode and an additional mode for $B>7$ T that grows in strength and splits with increasing field. A similar mode was also found in the corresponding single-particle excitations.[27] Here, this mode arises with the shifting of the ground-state density from $-3/2$ to primarily $+3/2$ character as described above.

The calculated FIR absorption for 14 holes in a QD based on a QW is shown in Fig. 6. Again we observe a nearly unchanged ω_- mode, a strongly lowered ω_+ mode with a splitting, and a new mode in the minus polarization related to the separation between the first HH and the first LH subband. The dipole spectrum for the QW system is significantly simpler than that for the HJ system in Fig. 5. As described above, the inversion symmetry in the z direction eliminates a part of the HH-LH couplings. Effects associated with this symmetry have been observed previously in 2DHG's.[59]

Within the investigated range from 6 to 14 holes per QD, the calculated FIR spectra show essentially no dependence on the particle number. For less than 6 holes per QD, we observe additional features, which might indicate the breakdown of our mean-field description. The spectra also do not exhibit a significant dependence on the temperature in the range of $T=0.1-4.2$ K. A repetition of our calculation in the Hartree approximation, neglecting the exchange-correlation corrections in the ground state and response calculations, results in different eigenenergies $E_{M\mu}$ and a slightly changed ground-state density profile, but gives essentially the same FIR absorption spectra.

In the high magnetic field limit, where the cyclotron orbit size becomes much smaller than the dot size, the influence of the Hartree and the exchange-correlation potential for the ground-state calculation as well as the influence of the depolarization and excitonic shift in Eq. (13) for the response calculation become negligible. In this limiting case the resonance energies are directly given by differences between eigenenergies $E_{M\mu}$ and our FIR absorption spectra become identical to those of a single hole in a QD, i.e., without interaction effects.[27] Furthermore, these spectra also approach the cyclotron resonance spectra of a corresponding 2DHG, calculated independently for the same QW or HJ parameters in a single-particle picture using also Luttinger's 4×4 $\mathbf{k}\cdot\mathbf{p}$ Hamiltonian.[60] (It should be noted that correlation effects anticipated in high magnetic field, such as Wigner crystallization, cannot be represented within our mean-field treatment). For the HJ system we also find good qualitative

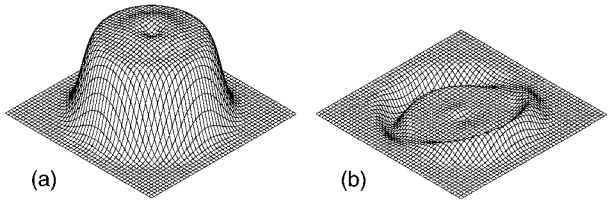

FIG. 7. (a) Same ground state density as in Fig. 1, and (b) the change of density for a rigid center-of-mass motion.

agreement with the available experimental cyclotron resonance data[33–35] of 2DHG's in $Ga_xAl_{1-x}As$-GaAs HJ's with the somewhat higher densities of $(2.7-5.6)\times 10^{11}$ cm^{-2} (compared to $\approx 1.5\times 10^{11}$ cm^{-2} for the areal density in the center of the QD with 14 holes). The high-field data (B = 10–14 T) are typically characterized by one main peak around 4 meV and one or two weaker features at slightly higher energy, as is the case for our calculated FIR spectra in Fig. 5.

For an interpretation of the modes in our absorption spectra we look at the form of the time-dependent induced change of the charge density as given by Eq. (20). According to the GKT, the only dipole active magnetoplasmon modes for electrons in parabolic QD's are c.m. motions. The corresponding rigid shifts of the ground-state density $n(\boldsymbol{\rho})$ are circular motions with the displacement vector

$$\delta\boldsymbol{\rho}_{\text{c.m.}}(t)=\delta\rho_0\begin{pmatrix}\cos(\alpha_0\pm\omega t)\\ \sin(\alpha_0\pm\omega t)\end{pmatrix}, \tag{23}$$

where $\delta\rho_0$ is the amplitude and α_0 the phase. The change in density $\delta n_{\text{c.m.}}(\boldsymbol{\rho},t)$ for a c.m. motion is therefore determined by

$$n(\boldsymbol{\rho})+\delta n_{\text{c.m.}}(\boldsymbol{\rho},t)=n[\boldsymbol{\rho}+\delta\boldsymbol{\rho}_{\text{c.m.}}(t)]. \tag{24}$$

A Taylor expansion for small amplitudes $\delta\rho_0$ of the right-hand side gives

$$\delta n_{\text{c.m.}}(\boldsymbol{\rho},t)=\delta\rho_0\frac{dn(\rho)}{d\rho}\cos(\alpha_0\pm\omega t-\varphi), \tag{25}$$

where $dn(\rho)/d\rho$ is the derivative of the ground-state density with respect to the radial coordinate. In Fig. 7 we plot the same ground-state density $n(\rho)$ as in Fig. 1 and the resulting $\delta n_{\text{c.m.}}(\boldsymbol{\rho},t)$ as given by Eq. (25). The change in density for a pure c.m. motion $\delta n_{\text{c.m.}}(\boldsymbol{\rho},t)$ can be compared with $\delta n(\boldsymbol{\rho},t)$ of Eq. (20) resulting from the response calculation. In the case of electrons in QD's [which we can describe by setting the HH-LH coupling terms R and S in Eq. (2) to zero] the calculated $\delta n(\boldsymbol{\rho},t)$ for the two modes $\omega_\pm$ in the spectrum of Fig. 4 reproduce the exact result $\delta n_{\text{c.m.}}(\boldsymbol{\rho},t)$ to a very high degree. But for holes a more complicated behavior is observed: in Fig. 8 we plot the real part of $\delta n(\boldsymbol{\rho},t)$ for selected resonances which are marked by grey triangles in the absorption spectrum of Fig. 5. Figures 7(a) and 7(b) and 8(a)–8(f) use the same length scale in the x-y plane, but the amplitudes are normalized to the same maximum height. According to Eq. (20) the time dependence of the density fluctuation patterns is given by a stiff rotation in polarization direction and with the frequency ω of the external dipole field. A comparison of Figs. 8(a)–8(f) with Fig. 7(b) shows that only the ω_- mode with Fig. 8(d) maintains a simple c.m. motion, whereas all other hole magnetoplasmon modes exhibit a mixture of c.m. and internal motion. The dipole excitation of such plasmon modes is according to the GKT not possible for electrons in parabolic QD's.

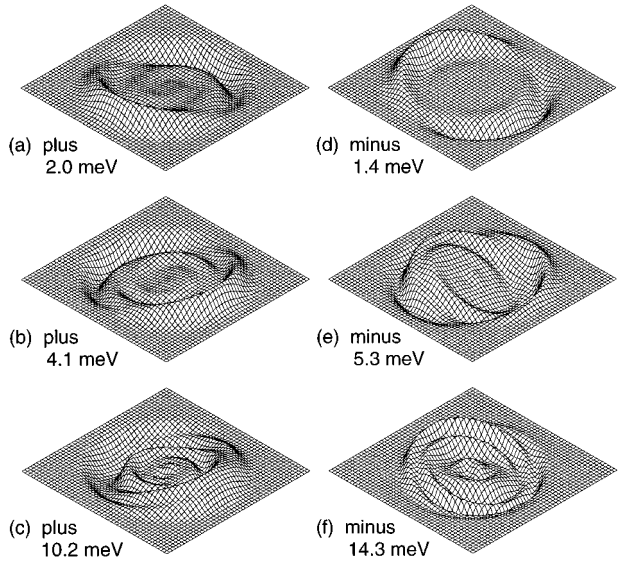

FIG. 8. Changes of the density for selected resonances marked with gray triangles in the absorption spectrum of Fig. 5. The plasmonic motions are given by a stiff rotation of these patterns in the polarization direction and with the frequency of the external field. The figures (a)–(f) are labeled by the polarization direction and the respective frequencies. These dipole induced plasmon motions exhibit strong deviations from a simple center-of-mass motion shown in Fig. 7(b).

VII. CONCLUSIONS

We have calculated the FIR absorption spectra of QD's confining holes, which reflect the dipole excitation of hole magnetoplasmons. The ground state of the many-hole system was determined in the LDA using Luttinger's 4×4 $\mathbf{k}\cdot\mathbf{p}$ Hamiltonian to include the valence-band mixing. The collective response to a dipole field was calculated within the RPA. We present the resulting FIR spectra for two realistic model systems: QD's with holes realized by the lateral modulation of a 2DHG in a $Ga_xAl_{1-x}As$-GaAs HJ or QW.

According to the GKT, parabolic QD's *with electrons* exhibit a single-particle dipole spectrum with the two resonance frequencies $\omega_\pm$, reflecting only magnetoplasmon modes with a rigid c.m. motion. For QD's *with holes*, the valence-band structure induces strong observable deviations from this simple behavior: the HH-LH mixing leads to a weak magnetic field dispersion of the ω_+ mode and to an anticrossing in this mode; the coupling of states evolving from different subbands in the z direction induces new dipole transitions at frequencies related to the energy separation between the lowest z states. The resonances in our calculated FIR absorption spectra are due to hole magnetoplasmon modes with *internal* motions of the charge density. The excitation of such modes is possible for holes in QD's as the dipole field couples also to the relative motion, but prohib-

ited by the GKT for electrons in QD's.

We hope that our results can stimulate the technical realization of QD's with holes in the near future.

ACKNOWLEDGMENTS

We are grateful to K. Kempa for valuable discussions on the RPA formalism and for providing a numerical routine. We thank R. Winkler for calculating cyclotron resonance spectra for comparable 2DHG's and for a critical reading of the manuscript. This work was performed with financial support from the Deutsche Forschungsgemeinschaft within the SFB 348, from the German Academic Exchange Service (DAAD) within the HSP II, and from the NATO Grant No. 920657.

[1] Ch. Sikorski and U. Merkt, Phys. Rev. Lett. **62**, 2164 (1989).
[2] T. Demel, D. Heitmann, P. Grambow, and K. Ploog, Phys. Rev. Lett. **64**, 788 (1990).
[3] A. Lorke, J. P. Kotthaus, and K. Ploog, Phys. Rev. Lett. **64**, 2559 (1990).
[4] J. Alsmeier, E. Batke, and J. P. Kotthaus, Phys. Rev. B **41**, 1699 (1990).
[5] B. Meurer, D. Heitmann, and K. Ploog, Phys. Rev. Lett. **68**, 1371 (1992).
[6] P. Junker, U. Kops, U. Merkt, T. Darnhofer, and U. Rössler, Phys. Rev. B **49**, 4794 (1994).
[7] V. Gudmundsson, A. Brataas, P. Grambow, B. Meurer, T. Kurth, and D. Heitmann, Phys. Rev. B **51**, 17744 (1995).
[8] W. Kohn, Phys. Rev. **123**, 1242 (1961).
[9] L. Brey, N. F. Johnson, and B. I. Halperin, Phys. Rev. B **40**, 10 647 (1989).
[10] P. Bakshi, D. A. Broido, and K. Kempa, Phys. Rev. B **42**, 7416 (1990).
[11] P. A. Maksym and T. Chakraborty, Phys. Rev. Lett. **65**, 108 (1990).
[12] U. Merkt, Ch. Sikorski, and J. Alsmeier, in *Spectroscopy of Semiconductor Microstructures*, edited by G. Fasol, A. Fasolino, and P. Lugli (Plenum, New York, 1989), p. 89.
[13] V. Fock, Z. Phys. **47**, 446 (1928).
[14] C. G. Darwin, Proc. Cambridge Philos. Soc. **27**, 86 (1931).
[15] D. Pfannkuche and R. Gerhardts, Phys. Rev. B **44**, 13132 (1991).
[16] D. Pfannkuche, R. Gerhardts, P. Maksym, and V. Gudmundsson, Physica B **189**, 6 (1993).
[17] D. Pfannkuche, V. Gudmundsson, and P. Maksym, Phys. Rev. B **47**, 2244 (1993).
[18] D. Pfannkuche, V. Gudmundsson, P. Hawrylak, and R. Gerhardts, Solid State Electron. **37**, 1221 (1994).
[19] D. A. Broido, K. Kempa, and P. Bakshi, Phys. Rev. B **42**, 11 400 (1990).
[20] V. Gudmundsson and R. Gerhardts, Phys. Rev. B **43**, 12 098 (1991).
[21] A. L. Fetter, Phys. Rev. B **33**, 5221 (1986).
[22] Z. L. Ye and E. Zaremba, Phys. Rev. B **50**, 17 217 (1994).
[23] U. Rössler, D. A. Broido, and F. Bolton, in *Low Dimensional Electronic Systems*, edited by F. Kuchar, G. Bauer, and H. Heinrich, Springer Series of Solid State Sciences Vol. 111 (Springer, Berlin, 1992), p. 21.
[24] T. Darnhofer and U. Rössler, Phys. Rev. B **47**, 16 020 (1993).
[25] W. Zawadzki and M. Kubisa, Semicond. Sci. Technol. **8**, S240 (1993).
[26] D. A. Broido, A. Cros, and U. Rössler, Phys. Rev. B **45**, 11 395 (1992).
[27] T. Darnhofer, D. A. Broido, and U. Rössler, Phys. Rev. B **50**, 15 412 (1994).
[28] T. Darnhofer, U. Rössler, and D. A. Broido, Phys. Rev. B **52**, 14 376 (1995).
[29] J. M. Luttinger, Phys. Rev. **102**, 1030 (1956).
[30] K. Suzuki and J. C. Hensel, Phys. Rev. B **9**, 4184 (1974).
[31] J. C. Hensel and K. Suzuki, Phys. Rev. B **9**, 4219 (1974).
[32] H. R. Trebin, U. Rössler, and R. Ranvaud, Phys. Rev. B **20**, 686 (1979).
[33] H. L. Störmer, Z. Schlesinger, A. Chang, D. C. Tsui, A. C. Gossard, and W. Wiegmann, Phys. Rev. Lett. **51**, 126 (1983).
[34] Z. Schlesinger, S. J. Allen, Y. Yafet, A. C. Gossard, and W. Wiegmann, Phys. Rev. B **32**, 5231 (1985).
[35] G. Kalinka, F. Kuchar, R. Meisels, E. Bangert, W. Heuring, G. Weimann, and W. Schlapp, in *High Magnetic Fields in Semiconductor Physics III*, edited by G. Landwehr, Springer Series of Solid State Sciences Vol. 101 (Springer, Berlin, 1992), p. 567.
[36] D. A. Broido and L. J. Sham, Phys. Rev. B **31**, 888 (1985).
[37] E. Bangert and G. Landwehr, Superlattices Microstruct. **1**, 363 (1985).
[38] E. Bangert and G. Landwehr, Surf. Sci. **170**, 593 (1986).
[39] U. Ekenberg and M. Altarelli, Phys. Rev. B **32**, 3712 (1985).
[40] U. Ekenberg, Surf. Sci. **170**, 593 (1986).
[41] C. M. Engelhardt, D. Többen, M. Aschauer, F. Schäffler, G. Abstreiter, and E. Gornik, Solid State Electron. **37**, 949 (1994).
[42] S. L. Wong, D. Kinder, R. J. Nicholas, T. E. Whall, and R. Kubiak, Phys. Rev. B **51**, 13499 (1995).
[43] M. Merkler, R. Winkler, T. Darnhofer, and U. Rössler, in *High Magnetic Fields in the Physics of Semiconductors*, edited by D. Heiman (World Scientific, Singapore 1995), p. 624.
[44] R. Winkler, M. Merkler, T. Darnhofer, and U. Rössler, Phys. Rev. B **53**, 10 858 (1996).
[45] S. R. E. Yang and A. H. MacDonald, Phys. Rev. B **41**, 1294 (1990).
[46] A. Kumar, S. E. Laux, and F. Stern, Phys. Rev. B **42**, 5166 (1990).
[47] K. Lier and R. R. Gerhardts, Phys. Rev. B **48**, 14 416 (1993).
[48] D. A. Broido (unpublished).
[49] C. Cohen-Tannoudji, B. Diu, F. Laloë, *Quantum Mechanics* (Wiley, New York, 1977), p. 727.
[50] W. O. G. Schmitt, Phys. Rev. B **50**, 15 221 (1994); **50**, 15 239 (1994).
[51] M. Jonson, J. Phys. C **9**, 3055 (1976).
[52] A. Zangwill and P. Soven, Phys. Rev. A **21**, 1561 (1980).
[53] *Intrinsic Properties of Group IV Elements and III-V, II-VI, and I-VII Compounds*, edited by O. Madelung, Landolt-Börnstein,

New Series Group III, Vol. 22, Pt. a (Springer, Berlin, 1987).
[54] F. Stern, Phys. Rev. B **5**, 4891 (1972).
[55] T. Ando, A. B. Fowler, and F. Stern, Rev. Mod. Phys. **54**, 437 (1982).
[56] J. F. Dobson, Phys. Rev. Lett. **73**, 2244 (1994).
[57] G. Vignale, Phys. Rev. Lett. **74**, 3233 (1994).
[58] Here, we are labeling states loosely according to the character of their dominant component. The eigenstates are mixtures of all four components.
[59] J. P. Eisenstein, H. L. Störmer, V. Narayanamurti, A. C. Gossard, and W. Wiegmann, Phys. Rev. Lett. **53**, 2579 (1984).
[60] R. Winkler (private communication).